

Interfacial thermal resistance in amorphous Mo/Si structures: A molecular dynamics study

Weiwu Miao(苗未午), Hongyu He(贺虹羽), Yi Tao(陶毅), Qiong Wu(吴琼), Chao Wu(吴超), and Chenhan Liu(刘晨晗)

Citation: Chin. Phys. B, 2025, 34 (**10**): 106501. DOI: 10.1088/1674-1056/adf9ff
http://cpb.iphy.ac.cn; http://iopscience.iop.org/cpb

What follows is a list of articles you may be interested in

Lattice thermal conductivity switching via structural phase transition in ferromagnetic VI_3

Chao Wu(吴超) and Chenhan Liu(刘晨晗)
Chin. Phys. B, 2023, 32 (**5**): 056502. DOI: 10.1088/1674-1056/acb764

Effects of phonon bandgap on phonon-phonon scattering in ultrahigh thermal conductivity ϑ-phase TaN

Chao Wu(吴超) and Chenhan Liu(刘晨晗)
Chin. Phys. B, 2023, 32 (**4**): 046502. DOI: 10.1088/1674-1056/acb201

Thermal transport in twisted few-layer graphene

Min-Hua Wang(王敏华), Yue-E Xie(谢月娥), Yuan-Ping Chen(陈元平)
Chin. Phys. B, 2017, 26 (**11**): 116503. DOI: 10.1088/1674-1056/26/11/116503

Thermal conductivity of carbon nanoring linked graphene sheets:A molecular dynamics investigation

Gang Shi(石刚), Jianwei Zhang(张鉴炜), Yonglv He(贺雍律), Su Ju(鞠苏), Dazhi Jiang(江大志)
Chin. Phys. B, 2017, 26 (**10**): 106502. DOI: 10.1088/1674-1056/26/10/106502

Thermal transport properties of defective graphene： A molecular dynamics investigation

Yang Yu-Lin (杨宇霖), Lu Yu (卢宇)
Chin. Phys. B, 2014, 23 (**10**): 106501. DOI: 10.1088/1674-1056/23/10/106501

RAPID COMMUNICATION

Interfacial thermal resistance in amorphous Mo/Si structures: A molecular dynamics study

Weiwu Miao(苗未午)[1], Hongyu He(贺虹羽)[1,2], Yi Tao(陶毅)[3], Qiong Wu(吴琼)[1], Chao Wu(吴超)[4,†], and Chenhan Liu(刘晨晗)[1,2,‡]

[1] *Advanced Thermal Management Technology and Functional Materials Laboratory, School of Energy and Mechanical Engineering, Nanjing Normal University, Nanjing* 210023, *China*

[2] *Ministry of Education Key Laboratory of NSLSCS, Nanjing Normal University, Nanjing* 210023, *China*

[3] *Jiangsu Key Laboratory for Design and Manufacture of Micro-Nano Biomedical Instruments, School of Mechanical Engineering, Southeast University, Nanjing* 211100, *China*

[4] *School of Electrical and Automation Engineering, Nanjing Normal University, Nanjing* 210023, *China*

(Received 25 June 2025; revised manuscript received 6 August 2025; accepted manuscript online 11 August 2025)

Efficient thermal management is critical to the reliability and performance of nanoscale electronic and photonic devices, particularly those incorporating multilayer structures. In this study, non-equilibrium molecular dynamics simulations were conducted to systematically investigate the effects of temperature, penetration depth, and Si layer thickness on the interfacial thermal resistance (ITR) in nanometer-scale Mo/Si multilayers, widely employed in extreme ultraviolet lithography. The results indicate that: (i) temperature variations exert a negligible influence on the ITR of amorphous Mo/Si interfaces, which remains stable across the range of 200–900 K; (ii) increasing penetration depth enhances the overlap of phonon density of states, thereby significantly reducing ITR; (iii) the ITR decreases with increasing Si thickness up to 4.2 nm due to quasi-ballistic phonon transport, but rises again as phonon scattering becomes more pronounced at larger thicknesses. This study provides quantitative insights into heat transfer mechanisms at amorphous interfaces and also offers a feasible strategy for tailoring interfacial thermal transport through structural design.

Keywords: thermal management, Mo/Si structure, interface thermal resistance, molecular dynamics simulation

PACS: 65.80.–g, 65.60.+a, 63.22.–m

DOI: 10.1088/1674-1056/adf9ff **CSTR:** 32038.14.CPB.adf9ff

1. Introduction

The rapid advancement of the semiconductor industry has driven the need for increasingly precise and efficient fabrication technologies. Among them, extreme ultraviolet (EUV) lithography has emerged as a core technique for next-generation nanoscale integrated circuits.[1–3] Multilayer optical mirrors, particularly those made from molybdenum/silicon (Mo/Si) films, are commonly used in EUV lithography systems because of their excellent reflective performance at EUV wavelengths.[4,5] However, as device dimensions shrink and power densities increase, the thermal management of these multilayer systems becomes a critical challenge. In particular, interfacial thermal resistance (ITR) between Mo and Si layers plays a pivotal role in governing the efficiency, reliability, and long-term stability of the optical system.[6] A thorough understanding of the thermal behavior at the Mo/Si interface is therefore essential for optimizing the performance of EUV lithography.

Phonons, the quantized vibrations of atoms, are the primary carriers of heat in non-metallic solids. When encountering an interface, phonons undergo reflection, transmission, and mode conversion, thereby affecting thermal transport efficiency across material boundaries[7,8] and leading to ITR. In amorphous materials, the lack of long-range atomic order results in localized vibrational modes, which are generally classified as propagons, diffusons, and locons.[9] These modes differ significantly from those in crystalline materials, where heat conduction is dominated by extended, coherent phonon modes. As demonstrated by Tian *et al.*,[10] the introduction of amorphous interlayers can increase inelastic phonon scattering and open new thermal transport channels, thereby reducing ITR. Compared to crystalline-crystalline interfaces, amorphous-amorphous interfaces exhibit more complex phonon behavior, making thermal transport mechanisms fundamentally different.[11] While considerable efforts have focused on crystalline systems,[12–14] studies on amorphous interfaces are scarce due to their intrinsically low thermal conductivity and indistinct temperature variation at the interfaces, thereby complicating both experimental measurements and theoretical modeling.[15,16] Nevertheless, interface struc-

†Corresponding author. E-mail: wuchao@njnu.edu.cn

‡Corresponding author. E-mail: chenhanliu@njnu.edu.cn

© 2025 Chinese Physical Society and IOP Publishing Ltd. All rights, including for text and data mining, AI training, and similar technologies, are reserved.

ture plays a key role, as highlighted by Bajt *et al.*,[4] who showed that a smoother interface can enhance both reflectivity and thermal stability in Mo/Si multilayers. Wei *et al.*[17] summarized the significant progress made in recent years in thermal interface materials (TIMs) in terms of enhancing thermal conductivity, reducing thermal resistance, and improving environmental sustainability. They also speculated that future developments in TIMs will focus on high performance, multifunctionality, intelligence, and sustainability. Considering that mismatch across the interface in Mo/Si structures leads to inefficient heat dissipation, thermal stress accumulation, and potential material degradation,[18] and the growing use of amorphous Mo/Si structures in nanoscale devices including thin-film solar cells,[19] high-power laser systems,[20] and efficient thermal management materials,[21] understanding the impact of interfacial structure on ITR is becoming increasingly important. However, this remains a largely unexplored issue, which this study aims to address.

In this work, we employ nonequilibrium molecular dynamics (NEMD) simulations to systematically investigate the ITR of amorphous Mo/Si structures under various conditions, including different penetration depths, temperatures, and layer thicknesses. Here, the penetration depth refers to the thickness of the interfacial region where the Mo and Si atoms intermingle. Our results indicate that the penetration depth has a significant impact on ITR, with an increasing penetration depth leading to a reduction in ITR. Phonon density of states (DOS) and its overlap analysis were employed to explain the changes in ITR. Furthermore, we found that the thicker Si layer in the Mo/Si structure reduces ITR due to the availability of more phonon transport modes. This study provides new insights into thermal transport characteristics at amorphous interfaces and offers practical guidance for enhancing the heat dissipation performance of Mo/Si multilayer systems in advanced electronic and photonic applications.

2. Simulation details

2.1. Model setup

In this study, molecular dynamics (MD) simulations were conducted using LAMMPS.[22] Atomic positions were integrated using the velocity Verlet algorithm, with a time step of 1 fs for the Mo/Si system. The visualization of the simulation system was generated using Ovito software.[23] The atomic interactions in amorphous Si and Mo structures were simulated using the Tersoff potential[24] and the modified embedded atom method (MEAM) potential,[25] respectively. In addition, for the interactions between Si and Mo atoms, the MEAM potential was used, with parameters provided in Ref. [26].

The amorphous Mo/Si structure generated in this study was obtained by first maintaining the single-crystal Mo/Si structure at 3000 K in the NPT ensemble under a pressure of 100 bar for 200 ps. The pressure was then reduced to 1 bar and held for another 200 ps. Finally, the system was relaxed at 300 K in the NVT ensemble for 200 ps. The penetration depth is defined as the effective thickness of the interfacial region where Mo and Si atoms intermingle and interact, quantified by the degree of overlap in their atomic positions. Figures 1(a)–1(c) show the interfacial structures corresponding

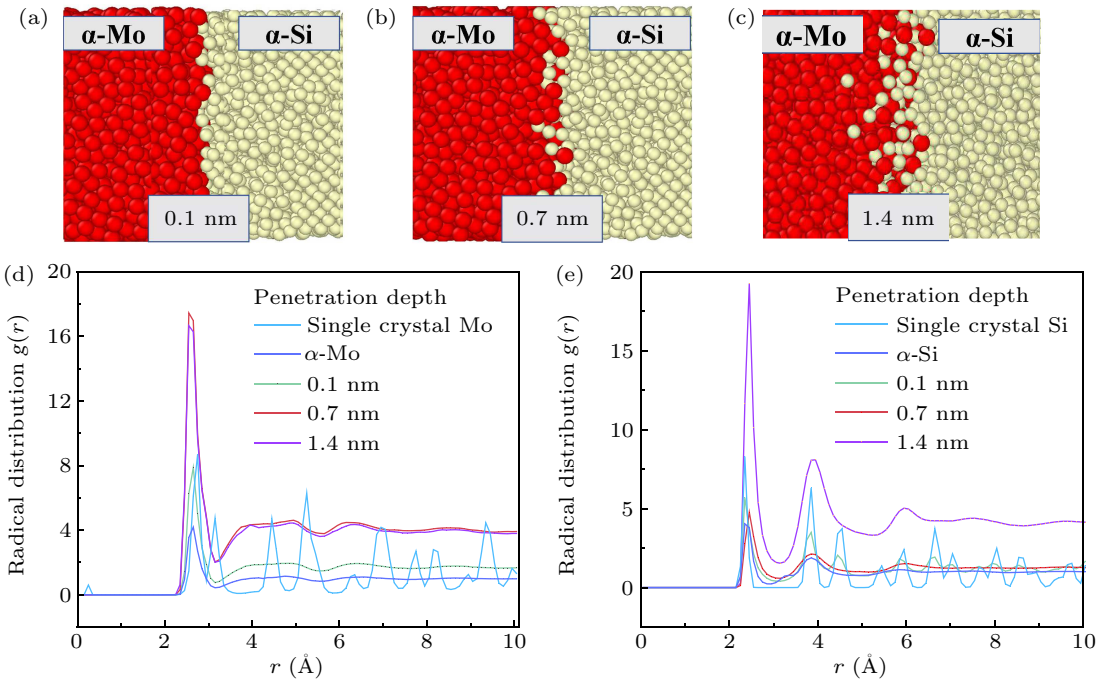


Fig. 1. Atomic information of the amorphous Mo/Si structure. Structures with penetration depths of (a) 0.1 nm, (b) 0.7 nm, and (c) 1.4 nm, along with the RDFs between (d) Mo–Mo atoms and (e) Si–Si atoms corresponding to these penetration depths.

to penetration depths of 0.1 nm, 0.4 nm, and 1.4 nm, respectively. To verify whether the simulated structures are amorphous, we calculated the radial distribution function (RDF) using the built-in $g(r)$ function of visual molecular dynamics (VMD) software for the single-crystal structure and structures with penetration depths of 0.1 nm, 0.7 nm, and 1.4 nm.[27,28]

Crystalline materials feature highly ordered atomic structures, as shown by the light blue lines in Figs. 1(d) and 1(e), where the RDF curves display sharp and regular peaks at specific distances, indicating well-defined atomic spacing and high probabilities of atomic pair occurrence.[29] Moreover, crystalline materials exhibit long-range order, with the RDF curve still exhibiting distinct peaks at larger interatomic distances.[29] In contrast, the atomic arrangement in amorphous materials is disordered. The randomness in atomic spacing leads to a more dispersed probability distribution of atomic pairs, resulting in a smoother RDF curve. As shown in a previous study,[30] amorphous structures exhibit only short-range order, meaning their atomic arrangement is orderly only within a few atomic spacings. Consequently, the intensity of RDF peaks rapidly decreases with increasing distance and eventually levels off. The curves in Figs. 1(d) and 1(e) clearly confirm the amorphous nature of the structures.[31]

2.2. Calculation methods

By applying periodic boundary conditions along both the x and y directions and fixed boundary conditions along the z direction, the ITR between amorphous Si and Mo was calculated using NEMD. Each simulation system has a total length of 151 Å along the z direction, which is perpendicular to the interface. To simulate the heat flux, hot and cold baths were placed at the two ends of the system. After the system reached a steady state, as described in Refs. [32,33], the heat flux density q and the temperature distribution were averaged over 10 ns to calculate ITR. The heat flux density q is calculated using the following formula:

$$q = \frac{\mathrm{d}E/\mathrm{d}t}{A}, \tag{1}$$

where $\mathrm{d}E/\mathrm{d}t$ represents the rate of energy supplied to or extracted from the system, and A is the area through which the heat flux passes. ITR is expressed in units of $(\mathrm{m}^2\cdot\mathrm{K})/\mathrm{W}$, representing the ratio of the temperature difference ΔT to the heat flux density

$$R_{\mathrm{ITR}} = \frac{\Delta T}{q}. \tag{2}$$

Based on these results, we further analyzed the relationship between ITR and penetration depth by examining DOS curves. The DOS in this study was calculated using velocity trajectory data obtained from molecular dynamics simulations in LAMMPS. It was obtained by performing a Fourier transform on the velocity autocorrelation function (VACF)[34]

$$\mathrm{DOS}(\omega) = \int \frac{\langle \sum_i v_i(t_0)\cdot v_i(t_0+t)\rangle}{\langle \sum_i v_i(t_0)\cdot v_i(t_0)\rangle} \mathrm{e}^{-2\pi \mathrm{i}\omega t}\,\mathrm{d}t. \tag{3}$$

Here, t_0 is the starting time and t is the correlation time. Building on previous studies by Li *et al.*[35] and Hajj *et al.*,[11] we introduced a parameter S to quantify the degree of DOS overlap, which was then used to analyze and explain variations in ITR, as shown in the following formula:

$$S = \frac{\int_0^\infty \mathrm{DOS}_1(\omega)\mathrm{DOS}_2(\omega)\,\mathrm{d}\omega}{\sqrt{\int_0^\infty \mathrm{DOS}_1^2(\omega)\,\mathrm{d}\omega}\sqrt{\int_0^\infty \mathrm{DOS}_2^2(\omega)\,\mathrm{d}\omega}}, \tag{4}$$

where ω is the frequency in units of Hz, and the subscripts 1 and 2 represent the left and right sides of the interface, respectively. In this study, within a 3 Å-thick region on both sides of the interface, 247 atoms from the Mo side and 249 atoms from the Si side were selected, and the DOS of each atom was calculated.

3. Results and discussion

3.1. The effect of temperature on interface thermal resistance

This section simulates the amorphous Mo/Si structure with a penetration depth of 0.1 nm and calculates its ITR over the temperature range from 200 K to 900 K. The simulation structure used is a Mo/Si/Mo structure, as shown in the schematic diagram in Fig. 2(a). The Mo/Si interfacial thermal resistance is calculated using the NEMD method, with Mo thickness set at 2.8 nm and Si thickness set at 4.2 nm, which corresponds to the highest reflectivity at the widely employed EUV wavelength of 13.5 nm. According to Eq. (1), calculating ITR requires determining the variables ΔT and $\mathrm{d}E/\mathrm{d}t$, as shown in Figs. 2(a) and 2(b). In Fig. 2(a), the Langevin thermostat method effectively establishes a linear temperature gradient inside the material by maintaining a fixed temperature at both ends of the Mo/Si/Mo system, so ΔT can be obtained from the sudden change at the interface. In Fig. 2(b), $\mathrm{d}E/\mathrm{d}t$ can be obtained from the linear fitting of the heat flux density versus time.

Figure 2(c) shows the variation of ITR with temperature. To minimize errors and ensure data reliability, we performed five independent simulations at each temperature with modified random seeds. The data in Fig. 2(c) represent the averaged results from these simulations, and the error bars represent the standard deviations. Although the value of ITR fluctuates at different temperatures, the overall change is minimal. Specifically, the interfacial thermal resistance is 15.17 $\mathrm{m}^2\cdot$K/GW at 200 K, 15.32 $\mathrm{m}^2\cdot$K/GW at 300 K, and 14.54 $\mathrm{m}^2\cdot$K/GW at 900 K, with a change of approximately 0.63 $\mathrm{m}^2\cdot$K/GW (less than 5%). The experimentally measured Mo/Si interfacial thermal resistance in Ref. [36] is 18.18 $\mathrm{m}^2\cdot$K/GW (dashed

line in Fig. 2(c)), which is close to our results, thereby validating our simulation. Overall, ITR in amorphous Mo/Si is insensitive to temperature between 200 K and 900 K.

According to Eq. (4), the parameter S was calculated at a penetration depth of 0.1 nm for different temperatures. As shown in Fig. 2(d), the value of S exhibits little variation with changing temperature. In general, a higher S value indicates better atomic arrangement compatibility between Mo and Si, reflecting a more periodic or spatially coherent atomic structure.[37,38] The similar values of S indicate that the atomic arrangement compatibility at the interface does not change significantly at different temperatures, consistent with the results in Fig. 2(c), which show that ITR changes only slightly and remains relatively stable across the temperature range of 200–900 K.

Additionally, we calculated and compared DOS at 300 K and 900 K, as indicated in Fig. 2(d). At higher temperatures, due to the increased atomic vibration frequencies, more high-frequency phonon states (high-energy phonons) are excited, causing the DOS to shift towards higher frequencies, and the high-frequency part of the phonon DOS curve becomes steeper.[39] At lower temperatures, low-frequency phonon states dominate, and the excitation of high-frequency states is limited, resulting in a flatter DOS curve in the low-frequency region.

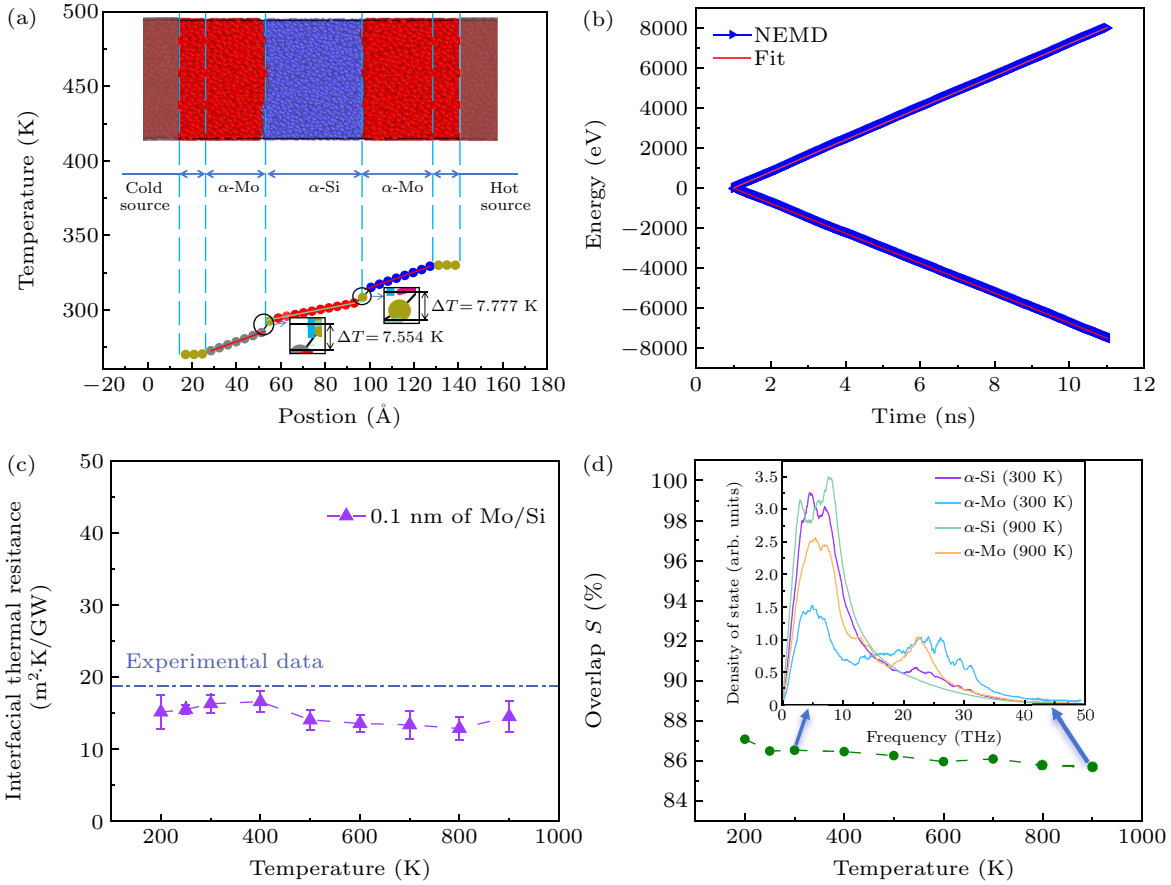


Fig. 2. Thermal properties of the Mo/Si structure with a penetration depth of 0.1 nm. (a) Temperature versus position at 300 K, with the atomic structure shown in the inset. (b) Time-dependent heat flux at 300 K. (c) Variation of interface thermal resistance with temperature. (d) DOS overlap parameter S at different temperatures. The inset shows the DOS.

3.2. The effect of penetration depth on interface thermal resistance

In this section, we analyze the variation in interface thermal resistance of Mo/Si as a function of penetration depth. The ITR was simulated five times at each temperature and penetration depth to ensure accuracy and reproducibility. Notably, Fig. 3(a) shows the variation of ITR with temperature at different penetration depths. At a penetration depth of 0.1 nm, the average ITR reaches its maximum value (16.61 m^2·K/GW), while as the penetration depth increases to 1.4 nm, it is significantly reduced to 3.59 m^2·K/GW, representing a reduction of more than 78%. Additionally, ITR decreases markedly with increasing penetration depth between 0.1 nm and 0.7 nm, while in the range from 1.0 nm to 1.4 nm, the decrease becomes relatively flat.

The monotonic decrease of ITR with increasing penetration depth indicates that the variation in ITR is closely related to the physical properties of the interface layer.[40] For example, Rane *et al.*[41] found that differences in lattice constants and thermal expansion coefficients between Mo and Si gen-

erate stress at the interface at small penetration depths. A shallow penetration depth indicates weaker interface bonding, which cannot effectively release stress, leading to stress concentration and defect formation. These interfacial defects enhance phonon scattering. Han *et al.*[42] further reported that enhanced phonon scattering intensifies non-equilibrium effects, resulting in thermal resistance that can exceed that caused by interfacial scattering alone. This significantly impedes heat transfer and leads to a pronounced increase in ITR. Xi *et al.*[43] recently proposed a universal thermal conductivity formula applicable to liquids, polymer glasses, and amorphous solids, with results in excellent agreement with experimental data. The simplified form of the formula is

$$\kappa = \alpha \frac{1}{\delta}\left(\frac{3}{2}+\frac{D_v}{2}\right)k_{\mathrm{B}}v_{\mathrm{s}}, \tag{5}$$

where α is the pre-factor for each state, δ is the distance between adjacent atoms or functional groups, and $(\frac{3}{2}+\frac{D_v}{2})k_{\mathrm{B}}$ is the high-temperature limit for the particle. In this study, as the penetration depth increases, the distance δ between Mo/Si atoms decreases. According to Eq. (5), the thermal conductivity thus increases, thereby reducing ITR, which is consistent with the trend observed in the simulation results.

Yang *et al.*[44] used the extended atomic Green's function method to study the interfacial thermal conductance (ITC) of amorphous interfaces and demonstrated that thermal conductivity can be enhanced by optimizing the atomic mass distribution within the amorphous interface. Their work confirmed that a gradient mass distribution strategy is effective for amorphous interfaces. In our study, at a penetration depth of 0.1 nm, the Mo/Si atomic interface can be approximated as a single atomic species. As the penetration depth increases, atoms from both the Si and Mo sides infiltrate into the other side, forming a structure similar to a gradient mass distribution. This effect contributes to the reduction in ITR.

Both elastic and inelastic scattering influence the overall ITR. Previous studies have found that elastic scattering plays a dominant role in determining the ITR of amorphous Mo/Si interfaces.[45] This dominance arises from the intrinsic atomic disorder at the interface, which enhances phonon scattering and makes the interface more susceptible to elastic interactions, while the contribution of inelastic processes is relatively small. Because the phonon DOS in amorphous materials is broader,[46] the energy exchange between phonons is less pronounced than in crystalline materials. Therefore, in amorphous Mo/Si structures, elastic scattering is the primary factor governing the variation of ITR.

The penetration depth defines the region where Mo and Si atoms overlap and interact at the interface, directly influencing the DOS by modifying the atomic interactions. As the penetration depth increases, the overlap of phonon states between Mo and Si atoms becomes larger, thereby altering the phonon distribution and overall DOS at the interface.[47] As shown in the inset of Fig. 3(b), when the penetration depth is 0.1 nm, the interaction between Mo and Si atoms in the interfacial region is limited, resulting in a small overlap of phonon states between the two materials. Consequently, the DOS exhibits sharper peaks, often at higher frequency ranges. With increasing penetration depth, the interaction between Mo and Si intensifies, leading to a greater phonon-state overlap. This causes a redistribution of the DOS, with an evident increase in the low-frequency region, while the high-frequency part shows relatively minor changes.

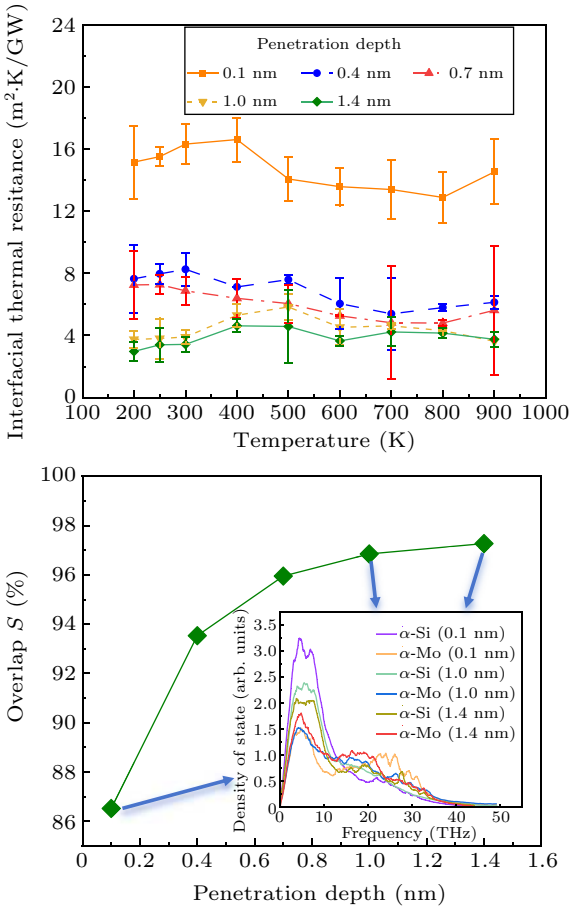


Fig. 3. Interfacial phonon properties of the Mo/Si structure. (a) Variation of ITR with temperature at different penetration depths. (b) DOS overlap parameter S for different penetration depths at 300 K. The inset shows the DOS.

The trend of ITR variation with penetration depth can be interpreted using the DOS overlap parameter S, as shown in Fig. 3(b). The detailed values of S for penetration depths of 0.1 nm, 0.4 nm, 0.7 nm, 1.0 nm, and 1.4 nm are 86.52%, 93.53%, 95.95%, 96.85%, and 97.27%, respectively. Since a larger S indicates greater similarity in phonon properties across the interface, the monotonically increasing trend of S explains the corresponding decrease in ITR. More importantly, the increase in S is significant within the 0.1–0.7 nm range but becomes marginal beyond 1.0 nm, which is consistent with the observed ITR behavior. Overall, as penetration depth in-

creases, ITR decreases monotonically due to the increasing similarity in phonon properties across the interface.

3.3. The effect of Mo/Si thickness on interface thermal resistance

This section uses the Mo/Si/Mo structure with a penetration depth of 0.1 nm as an example to investigate how interface thermal resistance varies with Si thickness.

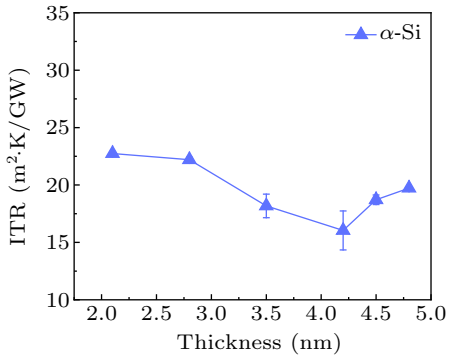


Fig. 4. Variation of interfacial thermal resistance with Si thickness in the Mo/Si/Mo structure, with the Mo layer fixed at 2.8 nm.

Figure 4 shows the relationship between the amorphous Si thickness and ITR. As the Si thickness increases from 2.1 nm to 4.2 nm, the ITR at room temperature monotonically decreases from 22.84 m^2·K/GW to 16.04 m^2·K/GW. However, for Si thicknesses greater than 4.2 nm, the ITR starts to rise again. For Si layers smaller than 4.2 nm, Hoegen *et al.*[48] found that in very thin Si layers, phonons may transport in a quasi-ballistic manner, highly sensitive to the interface properties. Larkin *et al.*[49] investigated the length of the propagator in α-Si, and the results showed that the wavelength of the typical propagator in α-Si is greater than 2 nm. When the thickness of amorphous Si is small (but still within the nanoscale), quasi-ballistic behavior dominates thermal conduction. In this regime, phonons are less likely to scatter at the interface, allowing heat to be transferred more effectively and thereby reducing the interfacial thermal resistance. Balasubramanian *et al.*[50] found that the difference in phonon propagation speed at the interface causes a mismatch in phonon frequencies. As a result, phonons passing through Si scatter at the interface, transferring only part of their energy to the other material. Such impedance to thermal transport results in a temperature discontinuity across the interface. They proposed a length-dependent theory, where, as the thickness increases, thermal transport transitions from ballistic transport at length scales smaller than the characteristic phonon mean free path (MFP) to diffusive transport in larger systems. The material thermal conductivity, which is a parameter in this relationship, also changes. They performed simulations and compared the results with Ref. [51], supporting this theory, which suggests that, for lengths smaller than the phonon mean free path, thermal resistance decreases as the distance increases. This can be interpreted as the increase in Si layer thickness leading to a greater number of phonon transport modes within the material. Similar results have been observed in previous studies on Si–Ge interfaces.[52] As a result, phonons are more likely to traverse the interface and enter the other material, which macroscopically manifests as a reduction in ITR.

For thicknesses greater than 4.2 nm, the ITR increases with layer thickness. Two factors contribute to this behavior. First, the critical point of the ITR variation in amorphous Si is related to the phonon mean free path (MFP). Once the thickness exceeds the phonon MFP, the thermal conductivity of the material becomes dominated by interface scattering.[53] Second, when the layer thickness exceeds the propagator length, the phonon propagation distance increases. In amorphous materials, structural disorder further enhances phonon scattering, causing the transport mode to gradually transition from quasi-ballistic to diffusive, which leads to an increase in ITR.[54]

Overall, in the Mo/Si structure with a penetration depth of 0.1 nm, the ITR decreases with increasing Si thickness up to 4.2 nm due to quasi-ballistic phonon transport, but increases again at larger thicknesses as phonon scattering becomes more pronounced.

4. Conclusion

In this study, molecular dynamics simulations were employed to investigate the ITR of amorphous Mo/Si structures over a temperature range of 200–900 K. The results demonstrate that temperature exerts a negligible influence on ITR, which remains stable across the entire range. A key finding is that increasing the penetration depth at the Mo/Si interface significantly reduces ITR, owing to enhanced atomic compatibility between the two materials. This interpretation is further supported by the observed increase in the DOS overlap. Moreover, increasing the Si layer thickness also reduces ITR, as the available phonon transport modes within the Si layer become more diverse. However, when the Si thickness exceeds 4.2 nm, phonon scattering becomes more pronounced, leading to an increase in ITR. In summary, this work provides quantitative insights into interfacial thermal transport in amorphous Mo/Si multilayer systems, which is essential for the design of EUV lithography optics and other advanced electronic and photonic devices.

Acknowledgments

This work was supported by the National Natural Science Foundation of China (Grant No. 52206092), the National Key R&D Program of China (Grant No. 2024YFF0508900), and the Big Data Computing Center of Southeast University as well as the Center for Fundamental and Interdisciplinary Sciences of Southeast University.

References

[1] Wu B and Kumar A 2014 *Appl. Phys. Rev.* **1** 011104
[2] Kazazis D, Santaclara J G, van Schoot J, Mochi I and Ekinci Y 2024 *Nat. Rev. Methods Primers* **4** 84
[3] Garner C M 2012 *Philos. Trans. R. Soc. A* **370** 4015
[4] Bajt S, Alameda J B, Barbee Jr T W, Clift W M, Folta J A, Kaufmann B and Spiller E A 2002 *Opt. Eng.* **41** 1797
[5] Andreev S, Salashchenko N, Suslov L, Yablonsky A and Zuev S Y 2001 *Nucl. Instrum. Methods Phys. Res. Sect. A* **470** 162
[6] Xing W, Xu Y, Song C and Deng T 2022 *Nanomaterials* **12** 3365
[7] Chen G 1999 *ASME J. Heat Transfer.* **121** 945
[8] Kosevich Y A, Potyomina L, Darinskii A and Strelnikov I 2018 *Phys. Rev. B* **97** 094117
[9] Allen P B, Feldman J L, Fabian J and Wooten F 1999 *Philos. Mag. B* **79** 1715
[10] Tian S, Wu T, Hu S, Ma D and Zhang L 2024 *Appl. Phys. Lett.* **124** 042202
[11] El Hajj J, Adessi C, de San Feliciano M, Ledoux G and Merabia S 2024 *Phys. Rev. B* **110** 115437
[12] Chen J, Xu X, Zhou J and Li B 2022 *Rev. Mod. Phys.* **94** 025002
[13] Inyushkin A, Taldenkov A, Ralchenko V, Bolshakov A, Koliadin A and Katrusha A 2018 *Phys. Rev. B* **97** 144305
[14] Wei L, Kuo P, Thomas R, Anthony T and Banholzer W 1993 *Phys. Rev. Lett.* **70** 3764
[15] Zhou W X, Cheng Y, Chen K Q, Xie G, Wang T and Zhang G 2020 *Adv. Funct. Mater.* **30** 1903829
[16] Zhu W, Zheng G, Cao S and He H 2018 *Sci. Rep.* **8** 10537
[17] Wei B, Luo W, Du J, Ding Y, Guo Y, Zhu G, Zhu Y and Li B 2024 *SusMat* **4** 239
[18] Yao Z, Stiglich J and Sudarshan T 1999 *J. Mater. Eng. Perform.* **8** 291
[19] Wei Z, Fung C M, Pockett A, Dunlop T O, McGettrick J D, Heard P J, Guy O J, Carnie M J, Sullivan J H and Watson T M 2018 *ACS Appl. Energy Mater.* **1** 2749
[20] Minasyan T, Ivanov R, Toyserkani E and Hussainova I 2021 *J. Alloys Compd.* **884** 161034
[21] Wu Y J, Sasaki M, Goto M, Fang L and Xu Y 2018 *ACS Appl. Nano Mater.* **1** 3355
[22] Thompson A P, Aktulga H M, Berger R, Bolintineanu D S, Brown W M, Crozier P S, In't Veld P J, Kohlmeyer A, Moore S G and Nguyen T D 2022 *Comput. Phys. Commun.* **271** 108171
[23] Stukowski A 2009 *Modell. Simul. Mater. Sci. Eng.* **18** 015012
[24] Tersoff J 1989 *Phys. Rev. B* **39** 5566
[25] Zhang X J, Zhang J M and Xu K W 2007 *Physica B* **391** 286
[26] Baskes M 1999 *Mater. Sci. Eng. A* **261** 165
[27] Chen J X, Bu L H, Liang Y C, Wang L Q and Ju X F 2011 *Harbin Gongye Daxue Xuebao (J. Harbin Inst. Technol.)* **43** 43
[28] Konnert J, D'Antonio P and Karle J 1980 *Adv. X-Ray Anal.* **24** 63
[29] Tian B, Ma W, Chen S, Sun F and Wang X 2024 *Int. J. Refract. Met. Hard Mater.* **119** 106560
[30] Cockayne D, McKenzie D, McBride W, Goringe C and McCulloch D 2000 *Microsc. Microanal.* **6** 329
[31] Lee B H, Larentzos J P, Brennan J K and Strachan A 2024 *npj Comput. Mater.* **10** 208
[32] Warzoha R J, Wilson A A, Donovan B F, Donmezer N, Giri A, Hopkins P E, Choi S, Pahinkar D, Shi J and Graham S 2021 *J. Electron. Packag.* **143** 020804
[33] Liu C, Chen W, Tao Y, Yang J and Chen Y 2018 *Int. J. Heat Mass Transfer* **121** 72
[34] Dickey J and Paskin A 1969 *Phys. Rev.* **188** 1407
[35] Li B, Lan J and Wang L 2005 *Phys. Rev. Lett.* **95** 104302
[36] Medvedev V, Yang J, Schmidt A, Yakshin A, Van de Kruijs R, Zoethout E and Bijkerk F 2015 *J. Appl. Phys.* **118** 085101
[37] Wei C, Zhang S, Wang Z, Zheng C, Peng B, Li C, Zhang Y, Li X and Cheng L 2022 *Compos. Part B: Eng.* **243** 110128
[38] Dharmawardhana C C, Zhou J, Taylor M, Miao J, Perepezko J H and Heinz H 2020 *Acta Mater.* **187** 93
[39] Shen G, Sturhahn W, Alph E, Zhao J, Tollenner T, Prakapenka V, Meng Y and Mao H R 2004 *Phys. Chem. Miner.* **31** 353
[40] Wu Y J, Zhan T, Hou Z, Fang L and Xu Y 2020 *Sci. Data* **7** 36
[41] Rane G K, Menzel S, Gemming T and Eckert J 2014 *Thin Solid Films* **571** 1
[42] Han J and Lee S 2024 *Phys. Rev. Mater.* **8** 014604
[43] Xi Q, Zhong J, He J, Xu X, Nakayama T, Wang Y, Liu J, Zhou J and Li B 2020 *Chin. Phys. Lett.* **37** 104401
[44] Yang L, Yang B and Li B 2023 *Phys. Rev. B* **108** 165303
[45] Gelin S, Tanaka H and Lemaître A 2016 *Nat. Mater.* **15** 1177
[46] Grimsditch M, Polian A and Vogelgesang R 2003 *J. Phys.: Condens. Matter* **15** S2335
[47] Keune W, Hong S, Hu M Y, Zhao J, Toellner T, Alp E E, Sturhahn W, Rahman T and Roldan Cuenya B 2018 *Phys. Rev. B* **98** 024308
[48] Hoegen H V 2024 *Struct. Dyn.* **11** 021301
[49] Larkin J M and McGaughey A J 2014 *Phys. Rev. B* **89** 144303
[50] Balasubramanian G and Puri I K 2011 *Appl. Phys. Lett.* **99** 013116
[51] Samvedi V and Tomar V 2009 *Nanotechnology* **20** 365701
[52] Tao Y, Liu C, Chen W, Cai S, Chen C, Wei Z, Bi K, Yang J and Chen Y 2017 *Phys. Lett. A* **381** 1899
[53] Song D, Jing D, Ma W and Zhang X 2019 *J. Appl. Phys.* **125** 015103
[54] Ishibe T, Okuhata R, Kaneko T, Yoshiya M, Nakashima S, Ishida A and Nakamura Y 2021 *Commun. Phys.* **4** 153